Available online at http://www.journalcra.com

International Journal of Current Research
Vol. 7, Issue, 07, pp. 18410-18421, July, 2015

INTERNATIONAL JOURNAL OF CURRENT RESEARCH

ISSN: 0975-833X

RESEARCH ARTICLE

THE CORROSION INHIBITION OF COPPER BY NEW ORGANIC COMPOUND $[(CH_3)_2N]_3PSe$ INTO CHLORIDE SOLUTION: ELECTROCHEMICAL STUDY

***,[1]Yafa Zargouni, [2,3]Wafa Sassi and [1]Khaled Alouani**

[1]Laboratoire de chimie analytique et d'électrochimie, Faculté des Sciences de Tunis, Université de Tunis-El-Manar, 2092, Tunisie
[2]Laboratoire de Mécanique-Énergétique, ENIT, Université de Tunis-El-Manar, BP 37, Tunis Belvédère, 1002, Tunisie
[3]Institut UTINAM, CNRS UMR 6213, Université de Franche-Comté, 16 Route de Gray 25030 Besançon, Cedex, France

ARTICLE INFO

Article History:
Received 13th April, 2015
Received in revised form
27th May, 2015
Accepted 30th June, 2015
Published online 31st July, 2015

Key words:
Copper, Corrosion,
Inhibitor, EQCM,
GDOES, EIS.

ABSTRACT

The corrosion inhibition properties of Tris-dimethyl-amino-seleno-phosphoramide (SeAP) for copper corrosion in NaCl solution were analyzed by electrochemical quartz crystal microbalance (EQCM) and potentiodynamic polarization. The morphological changes of copper were followed before and after adding SeAP, at different concentrations., by scanning electron microscopy (SEM), atomic force microscopy (AFM), and glow discharge optical emission spectroscopy (GDOES). The results show that SeAP acts by adsorption on copper via active sites and a protective layer formed on surface remains persistent over time in NaCl solution. The efficiency of SeAP increases with increase in immersion time into the chloride media.

Citation: Yafa Zargouni, Wafa Sassi and Khaled Alouani, 2015. "The corrosion inhibition of copper by New Organic Compound $[(CH_3)_2N]_3PSe$ into chloride Solution : Electrochemical study", *International Journal of Current Research*, 7, (7), 18410-18421.

INTRODUCTION

The use of organic inhibitors is one of the most practical methods to protect metals from corrosion, and is becoming of a great interest over decades as sited in some recent studies. The efficiency of organic inhibitors of corrosion mainly depends on their adsorption ability on metal surface, which can markedly change the corrosion resistance properties of metals (Ahamad and Quraishi, 2009; Kosari *et al.,* 2014; Li Xianghong *et al.,* 2014; Nam *et al.,* 2014; Ongun *et al.,* 2014). Therefore, understanding how the adsorption mechanism affects the corrosion inhibition is very important. For organic inhibitors, the adsorption at the metal/solution interface takes place through the replacement of water molecules according to the following equation (Bockris *et al.,* 1976):

$$Org_{(sol)} + x\ H_2O_{(ads)} = Org_{(ads)} + x\ H_2O_{(sol)} \quad \ldots\ldots\ldots\ldots\ldots\ (1)$$

Corresponding author: Yafa Zargouni,
Laboratoire de chimie analytique et d'électrochimie, Faculté des Sciences de Tunis, Université de Tunis-El-Manar, 2092, Tunisie.

In equation (1), $Org_{(sol)}$ and $Org_{(ads)}$ refer to organic molecule in solution and organic molecule adsorbed on metal surface, respectively. X is the number of water molecules replaced by organic molecules. As shown in several researches, the adsorption of organic molecules on metals surfaces depends on the nature and the surface charge of metals, the chemical structure of organic molecule (functional groups, steric factors, electron density, etc.) and the composition of solution used as chemical bath (FKhaled and Hackerman, 2003; Aljourani *et al*., 2009; Obot *et al.,* 2009; Fragoza-Mar *et al.,* 2012). The most effective and efficient inhibitors are the organic compounds that have heteroatoms with high electron density such as phosphorus, sulfur, nitrogen, oxygen or those containing multiple bonds (Solmaz *et al.,* 2011; Solmaz *et al.,* 2008; Chetouani *et al.,* 2003; Quraishi *et al.,* 2002; Abd El Maksoud, 2002; Doner *et al.,* 2013; Doner and Kardas, 2011; Yadav *et al.,* 2012). The presence of such atoms with high electron density and multiple bonds in molecular structure enhance the adsorption ability of organic compounds. Among the inhibitor compounds, the phosphorous compounds were known as efficient corrosion inhibitors for a variety of materials in acidic aqueous solutions.

In recent years, exhaustive practical experience has highlighted the importance of the phosphate in corrosion inhibition of copper and its alloys into acidic media (Song and Mansfeld, 2006; Kumaraguru *et al.,* 2006; Sowards and Mansfield, 2014; Tansuğ *et al.,* 2014; Hamani *et al.,* 2014; Zarrouk *et al.,* 2012; Pintado *et al.,* 2012). However, there is no study on how synthetic phosphorous compounds affect copper corrosion in sodium chloride solution. In this study, we aim to investigate the efficiency of a new synthesized organic phosphorous inhibitor Tris-dimethyl-amino-seleno-phosphoramide (SeAP) on copper (Cu) corrosion using electrochemical techniques and electrochemical impedance spectroscopy. The choice of this synthesized compound as an inhibitor was based on molecular structure considerations. SeAP molecule has three nitrogen atoms and one phosphorous atom, which are assumed to be an active center of adsorption.

Experimental Section

Materials and optimization

The inhibitor was synthesized according to the following procedure reported in the literature (Zargouni *et al.,* 2015). The purity of the SeAP was confirmed by NMR ^{1}H and NMR ^{13}P. The electrode rotation speed and the content of the SeAP into the chloride media are very important to optimize a resistant adsorbed layer against chloride ions penetration and to improve the corrosion inhibition in the shortest time possible. A Doehlert design, with $3^2 = 9$ experiment (3 levels and 2 factors), was carried out as a screening approach to optimize those experimental conditions using NEMROD software program (L. P. R. A. I, Marseille, France). The polarization resistance values Rp of Cu samples immersed into 3 wt.% NaCl and into 3 wt.% NaCl + SeAP used as responses in Doehlert design were investigated and described elsewhere (Zargouni *et al.,* 2015).

Fresh solutions of the 3 wt. % sodium chloride at pH of 7 were prepared for each experiment using analytical grade of pure NaCl and distilled water. The temperature was 20 ± 2°. The inhibitor concentration in the 3 wt. % NaCl corrosive media was achieved by adding aliquots of SeAP from a stock solution of 10 g dm^{-3}. The SeAP is not toxic within the range of concentration adopted. After adding the inhibitor to 3 wt. % NaCl solution, the measured pH of the mixture was 6.8.

Electrochemical potentiodynamic polarization

Electrochemical polarizations experiments were carried out in a three-electrode cell using a potentiostat–galvanostat Radiometer Copenhagen PGZ 402 model, piloted by Voltlab4 software. A saturated calomel electrode (SCE) was used as a reference electrode and a Pt electrode as a counter. Working electrodes (the tested samples) were prepared from rectangular coupons (1 cm²) of Copper. Before each test, the exposed surface of Cu samples was polished with 4000 SiC papers and washed with deionised water. The open circuit potential was stabilized within 60 min at room temperature. The cell was equipped so that the temperature during each experiment is kept constant.

Apparatus and methods

For electrochemical quartz crystal microbalance (EQCM) experiments, the working electrodes were a quartz crystal blade (6 MHz AT-cut) upon which a thin copper layer has been electroplated previously. The surface area of EQCM electrode was 1 cm^2. All additional information is described elsewhere (Sassi *et al*., 2014). For the gravimetric measurements, the results are presented as the mass variation with respect to time. The mass changes were derived from the observed frequency changes using the Sauerbrey equation (Sassi *et al.,* 2014):

$$\Delta f = - K_s \Delta m \quad \ldots\ldots\ldots\ldots\ldots\ldots \quad (2)$$

Where Δf is the frequency change, Δm mass change and K_s the constant depending upon the resonant frequency of the quartz. In this study, the nominal frequency was 6 MHz, K_s for the copper corrosion test was equal to 52 Hz μg^{-1} cm² according to the relative data of the EQCM instrument. The polarization curves and electrochemical impedance spectroscopy (EIS) were obtained by means of a potentiostat–galvanostat Radiometer Copenhagen PGZ 402 model, piloted by software Voltlab4. The test was a linear scan from E_1 cathodic potential (-1500 mV/SCE) to an anodic potential E_2 (500 mV/SCE) using a scanning rate of 25 mV/min. The polarization curves were plotted after 1800 seconds of immersion into the studied media (EQCM plots) to have reproducibility. The EIS experiments were realized in the frequency range from 100 kHz to 0.01 Hz at E_{ocp} with perturbation amplitude of 0.005 V peak-to-peak.

The surface topography and roughness of the samples were measured with a commercial Atomic Force Microscope (AFM PicoSPM from Molecular Imaging, USA). The experiments were conducted in air and at room temperature. The distribution of species in the deposit was determined by depth profiling with Glow discharge optical emission spectroscopy (GDOES) technique. The instrument was a Jobin Yvon GD-Profiler equipped with a 4mm diameter anode and operating after optimization at a pressure of 650 Pa and a power of 30W in an argon atmosphere. This low power was retained to decrease the speed of abrasion of the interfaces with low thickness and to obtain maximum information at the surface.

RESULTS AND DISCUSSION

In order to determine the optimum conditions related to the designed experiments on copper, we checked the evolution of R_p of the copper sample with the SeAP content (C_{SeAP}/mg L^{-1}) and the rotation speed (V_r /rpm) of the working electrode as shown in Fig.1. For this test, the optimum conditions relative to the highest R_p values were C_{SeAP} =2.8±0.1 mg L^{-1} and V_r = 3±1 rpm. Based on this result, we kept these values constant in all experiences.

EQCM and electrodeposition mechanisms

Fig. 2 presents the variation curves of the mass and the potential vs. time recorded for copper samples immersed into 3% NaCl solution before and after adding the SeAP.

The exam of Δm = f(t) on Fig.3-A, shows two different zones. The first zone is an increase of the mass gain (P-1) from 0 to 100 sec with a positive recorded Δm of about -0.4 µg cm^{-2}. Therefore, it seems to be the copper dissolution phase. Indeed, the jump amplitude of recorded potential values are about 50mV vs. SCE (Fig.2-A). This is well documented feature characteristic of surface passivation phenomena by formation of the "Cu_2O (cuprite)" passive film (Nilsson *et al.,* 2013; Zhaoa and Jiang, 2004). The second zone shows a decrease of the Δm values which falls until the end of the experience (Fig.2-A). The maximum mass lost recorded was 0.4 µg cm^{-2}. Moreover, Δm curve reveals the presence of four pseudo-plateaus (P-2, P-3 and P-4) related to fluctuations observed on potential versus time curve (Fig.2-A). A similar evolution of Δm has been related to the dissolution-passivation phenomena of copper into chloride media (Lilja *et al.,* 2013; Wu *et al.,* 2013).

Indeed, three main points should be explained. Firstly, the potential values recorded for NaCl + SeAP media are shifted to positive potentials compared to those obtained with SeAP free bath (Fig.2-B). These noble potentials could be due to the adsorption of SeAP compounds which seem acted on surface anodic sites. Indeed, many researches (Sassi *et al.,* 2012; Garza *et al.,* 2004; Simka *et al.,* 2013; Lee *et al.,* 2012; Ahmadi *et al.,* 2013) show that phosphorous based compounds act as anodic corrosion inhibitor of copper in chloride media. Secondly, the zone of copper oxide (Cu_2O) dissolution phase (P-1 and P-2 on Fig.3-A) has been removed from Fig.2-B. It has been suggested that the rate of organic molecules adsorption was faster than the passive film dissolution. In addition, the adsorption of organic compounds (observed on Δm curve, Fig.2-B) included two plateaus (P-2 and P-3) at about 870 and 1070 sec (Fig.2-B).

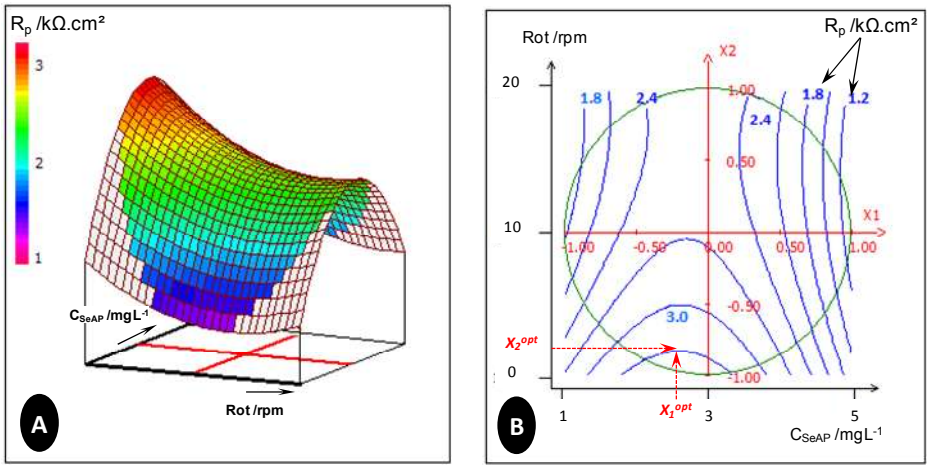

		X_i : Factors	
		X_1	X_2
Experimental field	Low limit (-)	1	0
	Upper limit (+)	5	20
Optima Conditions	X_i Optimum	2.8	3

Mathematical approach for the responses equation:

$Y = 21.5 - 5.2\,X_1 - 3.6\,X_2 + 8.9\,X_{12} - 7.6\,X_{22} - 0.2\,X_1X_2$

X_1 : C_{SeAP} ($mg.L^{-1}$) : SeAP content into the corrosive media.

X_2 : Rot (rpm) : electrode rotation speed.

Y : Rp ($k\Omega.cm^2$) : polarization resistance of the sample

Fig.1. Isoresponse curves for the modeling polarization resistance Rp ($k\Omega\ cm^2$) of copper substrate function of SeAP concentration (C_{SeAP}) and electrode rotation speed (V_r) into the corrosive media

Therefore, the first pseudo-plateaus (P-1 and P-2) observed on Δm curve and followed by a decrease and small fluctuations of potential values have been referred to the dissolution of the Cu_2O passive film products (Fig.2-A). Then, between 450 and 1000 seconds, the third and fourth pseudo-plateaus (P-3 and P-4) have been related to the compactness growth of the passive film when the potential values slightly shifted to noble values. Finally, the formation of soluble metal-chloride complexes is mentioned by a loss of sample mass (P-4 and P-5) and a stabilization of the open circuit potential values at around -220 mV/SCE. Fig.2-B, presents the evolution of potential and mass change vs. time corrosion of copper sample into 3% NaCl bath containing 2.8 mg L^{-1} of SeAP. The curve behavior is different from Fig.2-A.

Therefore, we had adsorption of two different adsorbates; SeAP molecules and SeAP-chloride complexes (justified further). Finally, potential curve shows many oscillations (Fig.2-B). Beyond 1100 seconds, the oscillations record important amplitude values of about 50 mV/SCE followed by two plateaus (P-4 and P-5) on Δm curve. Hence, this curve behavior has been referred to the growth of the adsorption of SeAP and related compounds. On the other hand, the last jump of potential value observed on Fig.2-B at around 1600 sec stabilizes at -135 mV vs SCE with stable Δm at around 2.45 µg cm^{-2}. Generally, the increase of mass gain of the Cu/SeAP system indicates an enhancement of the surface layer compactness and/or thickness. Therefore, the morphology of all samples should be considered.

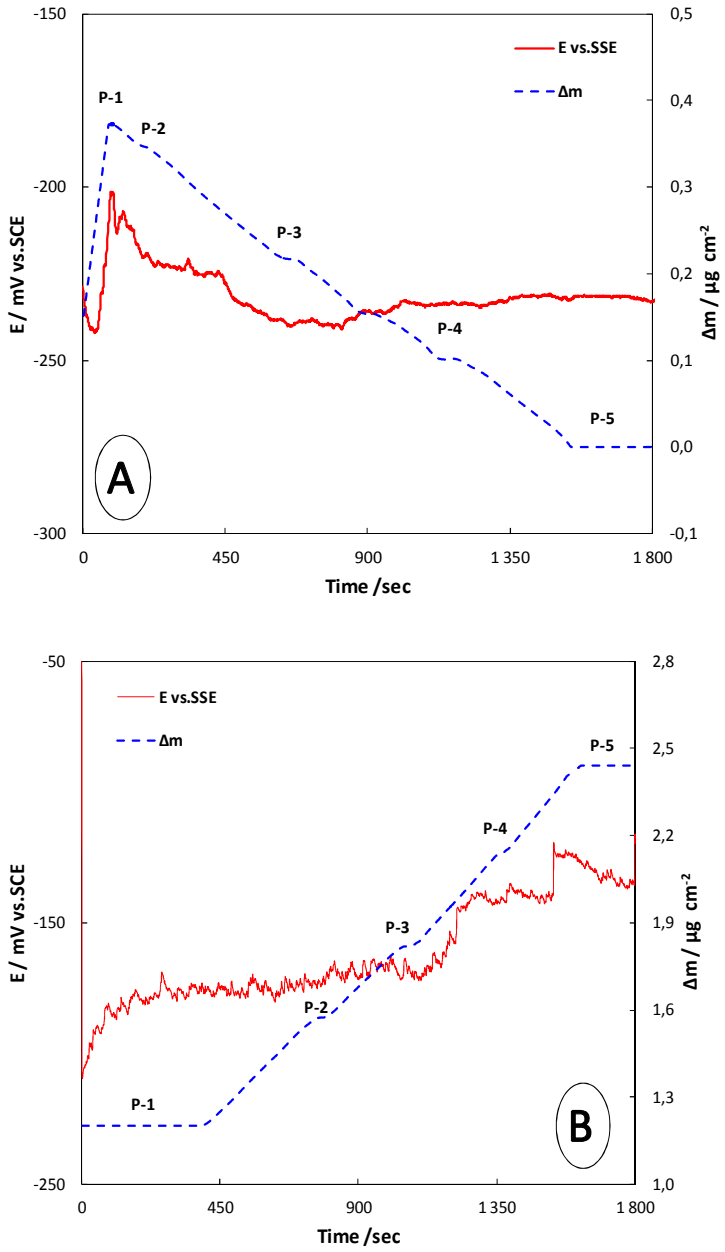

Fig.2. EQCM data on the mass and potential changes of the copper substrate into (A) NaCl and (B) NaCl + SeAP during open circuit potential

AFM and GDOES depth profile

After EQCM analysis, we took a set of 3D AFM images, gathered in Fig.3, for the tested samples. The surface roughness values estimated were 355 and 183 nm for copper immersed into 3% NaCl before and after adding SeAP, respectively. The copper surface after the treatment with SeAP seems to be smoother and a thick adsorbed film is present. One should also note the presence of bright dendrites on extreme surface on Fig.3-B related to the phosphorous based structure. Fig.4 showed a comparison of GDOES depth profile of oxygen and chloride incorporation into interface adsorbed film on copper surfaces. The contents of Na, C, N and H were removed from registered spectra to simplify the profile interpretation and to minimize the incertitude error of the wt. %.

Indeed, the adsorbed film on copper surface seems to be thicker (~ 10µm) when the SeAP was added to the corrosive media (Fig.3). However, the passive film on copper surface does not reach 2µm. This result is according to the AFM morphology observed in Fig. 3. The Fig.4-B show also that the content wt.% of phosphorus recorded is about 40 in the adsorbed film on Cu. Hence, it could be confirmed that the SeAP has been adsorbed on copper surface in both directions horizontally (totally covering the metallic surface) and vertically (enhancing the film thickness). This behavior is related to the copper affinity with organic compounds especially phosphorus inhibitors as mentioned elsewhere (Sassi *et al.,* 2012; Garza *et al.,* 2004; Simka *et al.,* 2013; Lee *et al.,* 2012; Ahmadi *et al.,* 2013). Moreover, chloride presence on the copper surface is the most important for sample immersed into free SeAP media (Fig. 4-A).

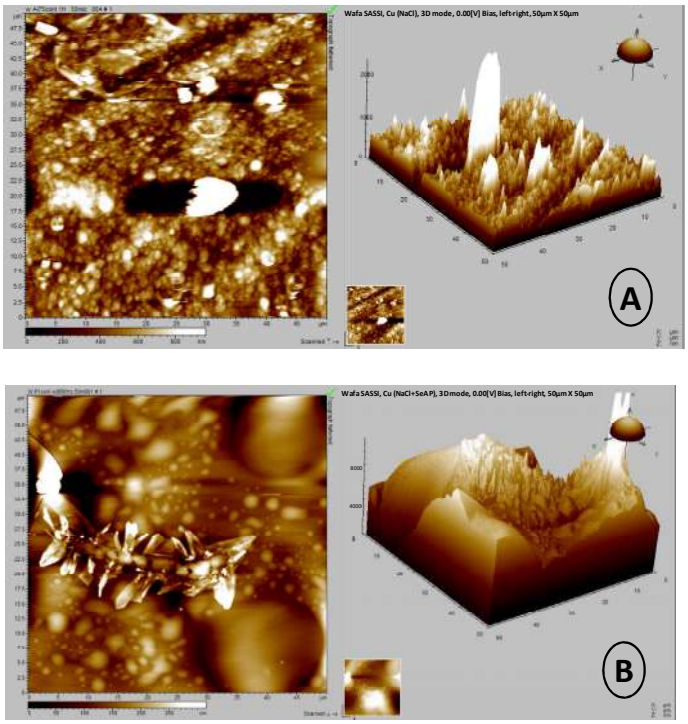

Fig.3. AFM 3D and tapping mode images of the copper substrate into (A) NaCl and (B) NaCl+SeAP after open circuit potential curve

Nevertheless, the slow chloride diffusion rate in the case of SeAP media could be referred to the low surface activity of the copper. Indeed, in the absence of the SeAP inhibitor, the chloride diffusion may deteriorate the Cu_2O passivation and accelerate the dissolution of the surface. This result could be confirmed by the presence of 5%wt. of oxygen on the extreme surface (Fig.4-A).

Polarization and SEM observations

The linear polarization curves of copper immersed into chloride media without and with addition of SeAP are gathered on Fig.5-A. The addition of SeAP into chloride media increases the immunity domain of copper. Moreover, the oxidation wall of copper at -80 mV/SCE had been removed after addition of the inhibitor compound. However, one should note the presence of the passivation peak (P_1) of copper sample immersed into 3% NaCl solution (at around -220mV/SCE on Fig. 5-A). The SEM micrograph on top of peak P_1 is shown on Fig.5. We could easily detect the presence of NaCl needles adsorbed on surface. Corrosion products are also detected and especially small cubic structures referred to Cu_2O oxides. The linear polarization curve and SEM micrograph prove that the increase of current density by oxidation of copper and formation of copper oxide "Cu_2O" are the cause of the appearance of the peak P_1. On the other hand, into 3% NaCl + SeAP media, the passivation peak (P_1) has been shifted to positive potential values at around -130mV/SCE and appears broad and less intensive (P_2 on Fig.5-A). The immunity domain of copper has been extended and the oxidation wall has been shifted beyond potential value 500 mV/SCE. The SEM micrograph on top of peak (P_2) is presented on Fig.5.

Indeed, the adsorption of SeAP compound is confirmed on copper surface by the presence of dendrites and ramification structures. One should also note, that compared to P_1 SEM micrograph, the substrate surface seems to be stable and no damages is observed. Nevertheless, some small cubes are detected and referred to the passive crystals of copper Cu_2O. Tafel presentation curves of copper obtained into chloride media with and without SeAP inhibitor are shown in Fig. 6-A. The cathodic corrosion reaction in a nearly neutral chloride solution for all samples is the reduction of water (Deng and Fu, 2012; Solmaz *et al.,* 2005):

$$2H_2O + 2e^- = H_2 + 2OH^- \quad \text{..... (3)}$$

However, in an aerated solution, the dissolved oxygen can destroy this protective hydrogen film that can be formed on the sample surface and oxidize the dissolved ions into insoluble forms (Solmaz *et al.,* 2007). Deposits of rust in a plumbing system are such an example of differential aeration cells and accelerated corrosion (Solmaz *et al.,* 2011; Solmaz *et al.,* 2008). For copper sample immersed into 3% NaCl+ SeAP, the potentiodynamic plot is shifted towards lower currents when compared to sample immersed into free inhibitor media. The cathodic branch of copper specimen reveals the reduction of water. The cathodic branch of NaCl +SeAP system reveals a Tafel slope corresponding to the simultaneous reduction of oxygen and protons H^+ (Li *et al.,* 2012; Solmaz *et al.,* 2005; Solmaz *et al.,* 2007; Solmaz *et al.,* 2011; Solmaz *et al.,* 2008). One should also note, that the cathodic current of curve obtained with SeAP addition is lower than that obtained from NaCl bath by a factor of 10.

The anodic branches can be divided to two regions, corresponding to the behavior of each of the samples. The corrosion potential value of NaCl + SeAP sample is shifted to positive values which could be referred to an enhancement of the corrosion resistance of the sample. The corrosion current density is lower than values recorded for the free SeAP media. However, passivation peaks of copper still present for the two curves. The morphology of both copper samples after potentiodynamic polarization were presented in Fig. 6-B and 6-C. Into 3% NaCl, the copper surface was heterogeneous, needles structure was destroyed into corrosive solution and deep pores were visible (Fig. 6-B). On the other hand, after polarization and at the first look, copper immersed into NaCl + SeAP inhibitor seems to be protected from chloride ions (Fig. 6-C). Nevertheless, one should note the presence of dendrites structure on Fig.6-C with some hairline cracks. At this zone, EDS studies reveal the presence of phosphorous and selenium (unreported results). Therefore, this structure has been referred to the presence of SeAP compounds adsorbed onto copper surface.

EIS measurements

In order to examine the mechanism of anodic and the cathodic reactions as well as the stability of the inhibitor film, EIS measurements were carried out. The obtained data are presented in Nyquist and Bode representations in Fig. 7. In addition, electrical parameters obtained by fitting the experimental results of EIS are gathered into Table 1.

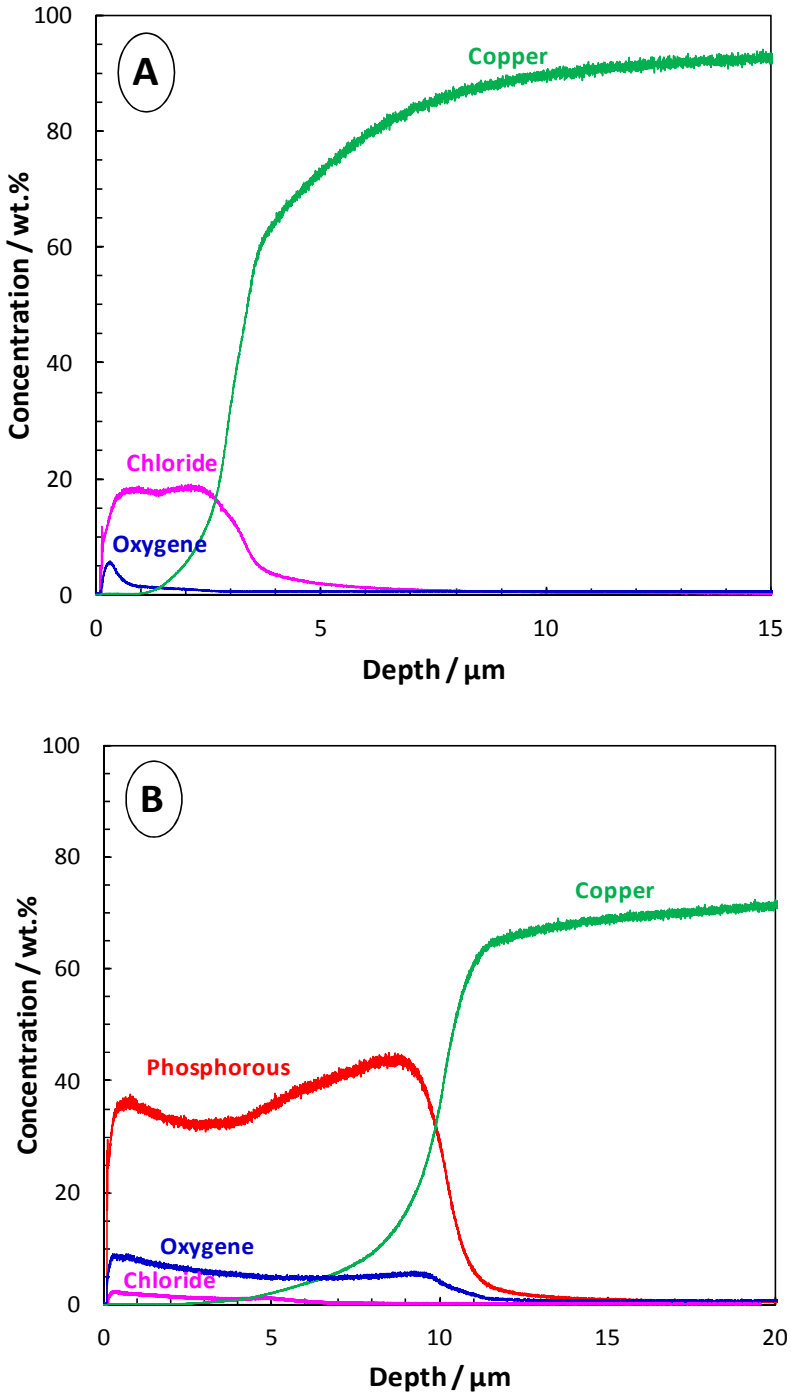

Fig.4. GDOES depth quantified profile of the copper substrate into (A) NaCl and (B) NaCl+SeAP after open circuit potential curve

The CPE element (constant phase element) is commonly converted into a pure capacitance (C_{eff}) by the means of the following equation (Orazem *et al.,* 2006):

$$C_{eff} = \frac{(CPE.R_2)^{1/\alpha}}{R_2} \quad \text{..... (4)}$$

After one hour immersion into 3% NaCl solution, Fig. 7-A shows that only one capacitive loop is observed suggesting that the reduction of the H^+ ions is charge transfer controlled (Solmaz *et al*., 2008; Orazem *et al*., 2006; Motamedi *et al.,* 2013; Behpour *et al.,* 2009).

Even after the increase of immersion time from 1h to 120h of copper sample, only one capacitive loop is observed (Fig.7-A). The similar behavior appears in the presence of the inhibitor (Fig. 7-B) indicates that the addition of SeAP to NaCl solution does not change the mechanism of the hydrogen evolution reaction. The inhibitor molecules adsorb on the copper surface, and block the reaction sites of the copper. This way, the surface area available for the H^+ ions decreases while the actual reaction mechanism remains unaffected (Li *et al.,* 2012; Solmaz *et al.,* 2005; Solmaz *et al.,* 2007; Solmaz *et al.,* 2008; Orazem *et al.,* 2006; Motamedi *et al.,* 2013;

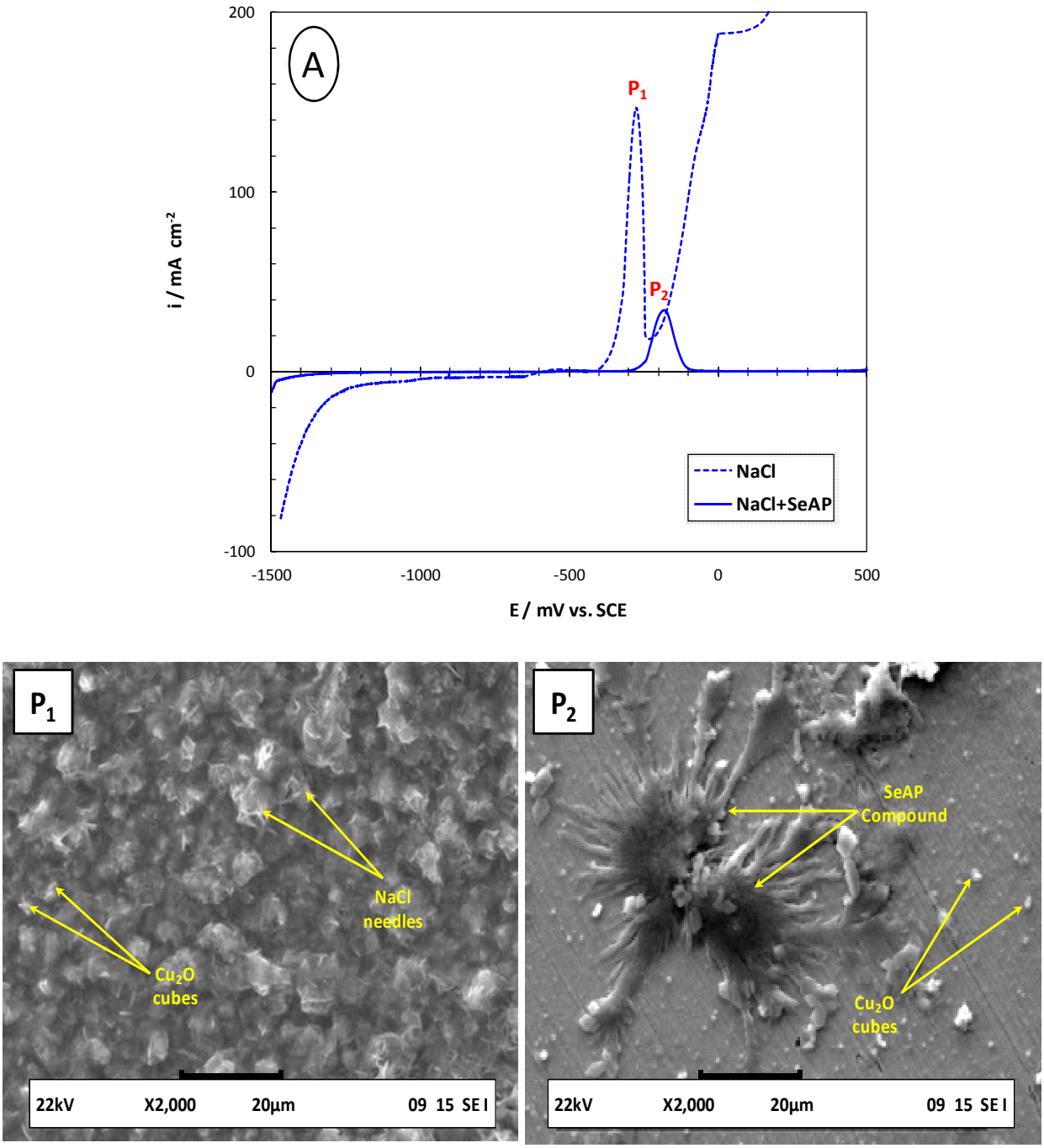

Fig.5. (A) Polarization curves of the copper substrate into NaCl and NaCl+SeAP, (B) and (C) SEM micrographs on top of peaks P_1 and P_2, respectively presented on Fig.5-A

Behpour *et al.,* 2009; Solmaz *et al.,* 2008; Keles *et al.,* 2008). The Rp values estimated after 120h from Bode plots by simulation are around 1.2 kΩ cm² and 3,9 kΩ cm² before and after adding the inhibitor, respectively. Fig. 7-D shows that the Bode plot of copper contains two time constants in the presence of the inhibitor. The first capacitive slope appeared at high frequency region is related to the charge transfer resistance and the double layer resistance, whereas a straight line at low frequencies is assigned to the diffusion process [38, 45]. Whereas, the Bode representation of the copper species into NaCl solution free SeAP (Fig.7-C) shows one time constant time at low frequencies related to the oxygen diffusion process.

On the other hand, the phase plots of copper, gathered on Fig.7-E, show one constant time related to the oxygen diffusion. However, Fig.7-F, related to the sample immersed 1h into NaCl+ SeAP solution, shows the presence of two constant times. This observation indicates that the inhibitor molecules have been adsorbed onto the metal surface and considerably reduced the dissolution rate of copper. One should note also, that the phase angle recorded at Fig.7-E and Fig.7-F are around 50°, 60° and 70° after 1h, 24h and 120h immersion into either NaCl or NaCl+ SeAP, respectively. Hence, the reach of the phase angle up to ~90 degrees with the increase of the immersion time indicate the decrease of the inhomogeneity of the surface samples.

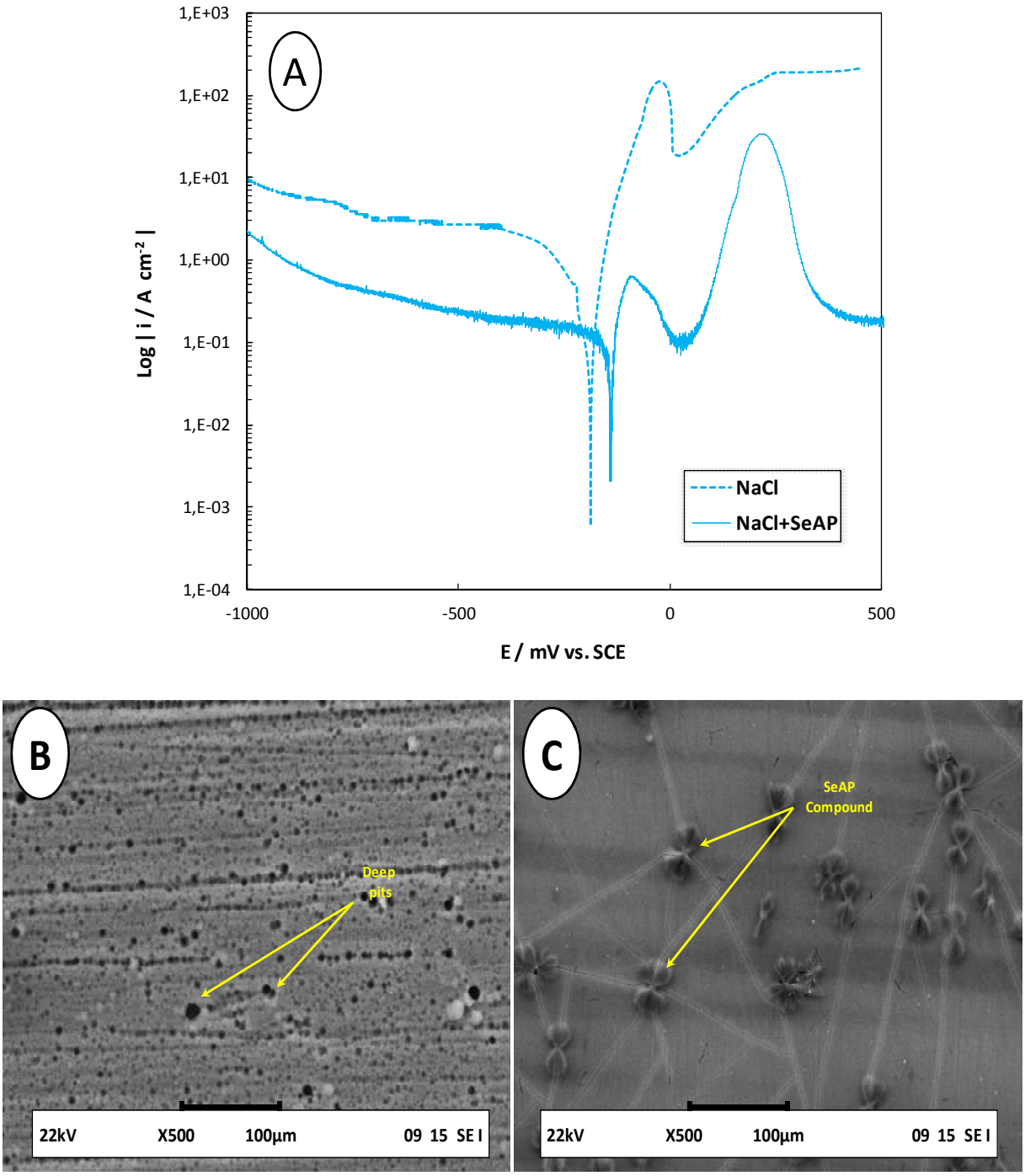

Fig.6. (A) Tafel presentation of curves shown in Fig.6-A, (B) and (C) SEM micrographs of the copper samples into NaCl and NaCl+SeAP, respectively and after polarization experiment

Indeed, this behavior could be referred to the saturation of extreme surface by corrosion products. Furthermore, the impedance diagrams were adequately modeled by equivalent electric circuit method illustrated in Fig. 8. In this equivalent circuit, instead of pure capacitors, constant phase elements (CPE) were introduced in the fitting procedure to obtain good agreement between the simulated and experimental data. The CPE represents the non-perfect capacitive response of the system and is well described elsewhere (Zargouni *et al.,* 2015; Sassi *et al.,* 2014; Sassi *et al.,* 2012).

The high frequency time constant (R_1, CPE_1) was attributed to the protective coating properties and it is represented by the pore resistance (R_1) and the capacitance of the film (CPE_1).

The second time constant including a charge transfer resistance and a double layer capacitance (R_2, CPE_2) simulates the behavior of the spectra at lower frequencies. The resistance of the solution is illustrated as R_e.

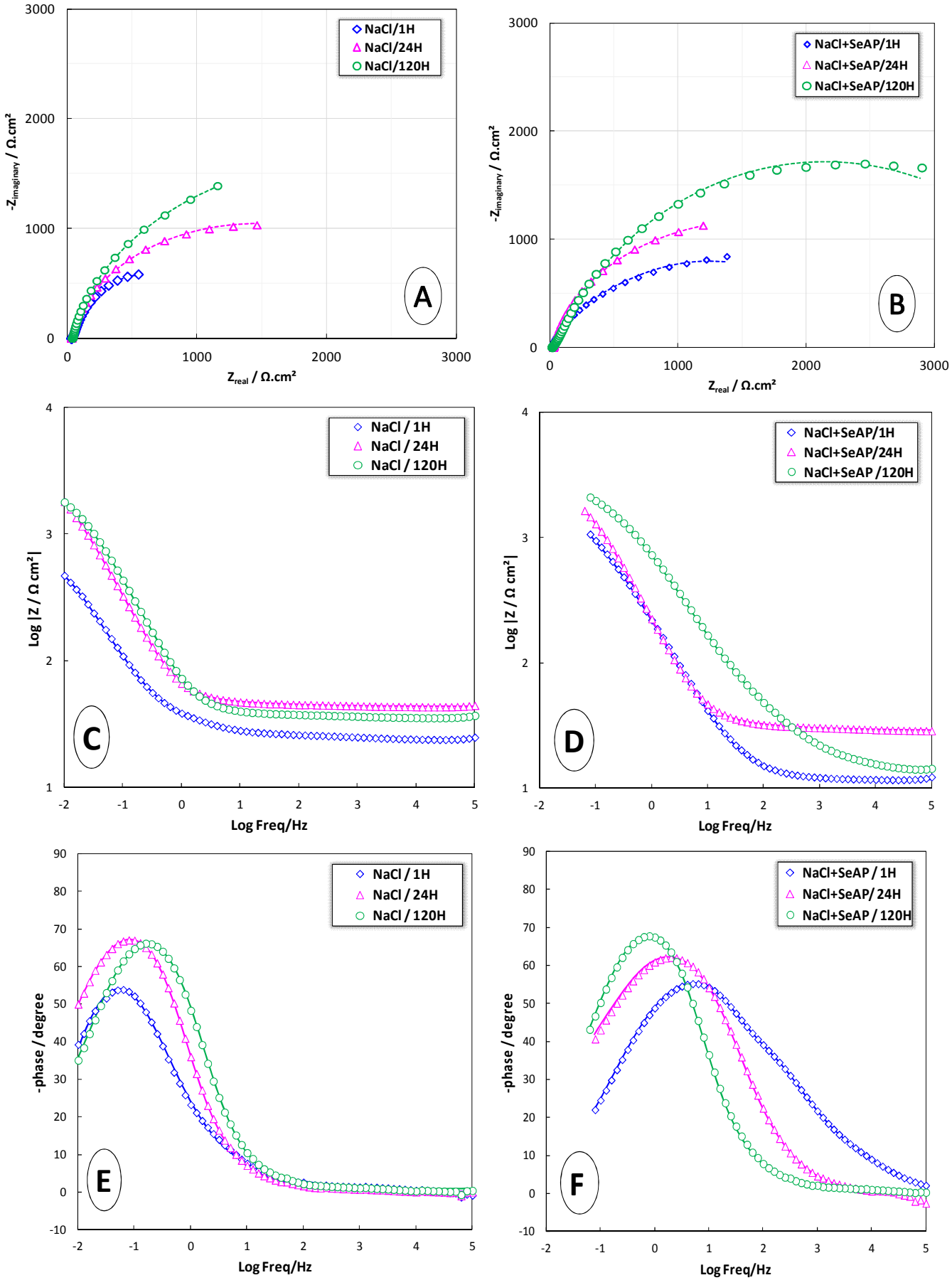

Fig.7. Nyquist, Bode and Phase plots of the copper samples after 1h, 24h and 120h immersion into NaCl and NaCl+SeAP media

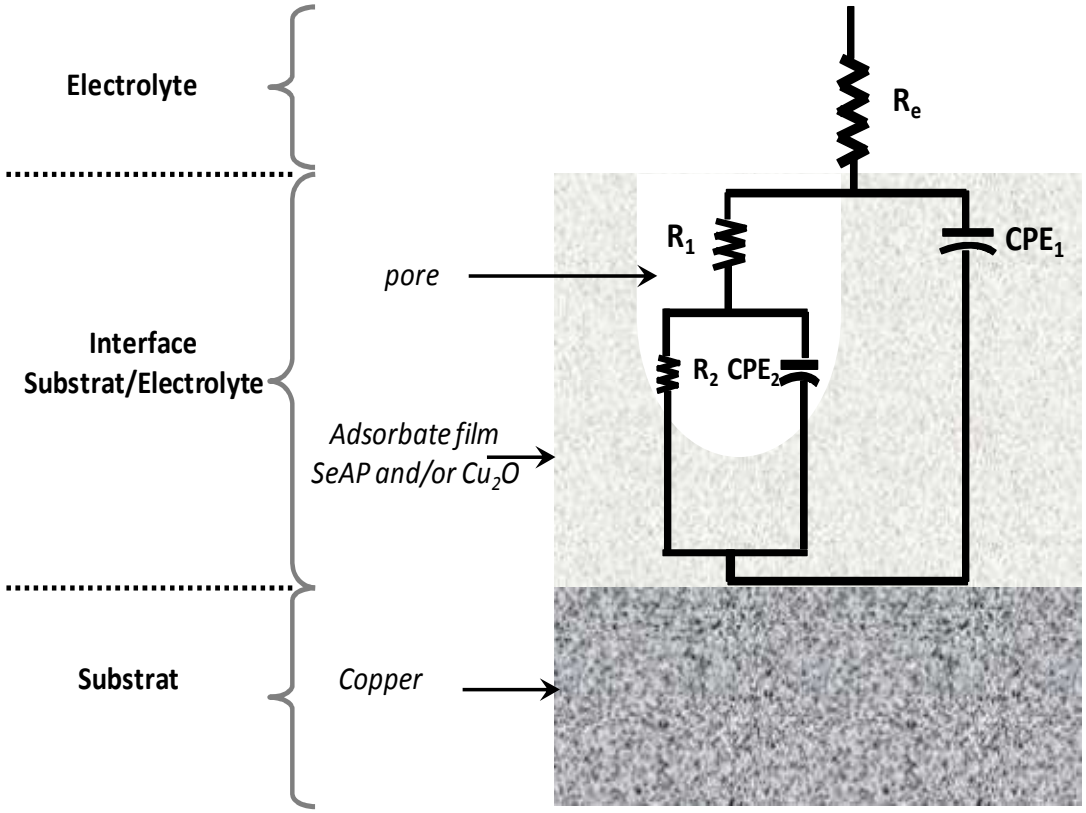

Fig. 8. Equivalent circuit used to identify and fit the EIS results of copper samples systems

Conclusion

The corrosion inhibition mechanism and the stability of SeAP on copper in 3% NaCl solution were investigated. The SEM and AFM studies show that the SeAP molecules evenly distribute over the copper surface. Moreover, the anodic effect of SeAP is better than its cathodic one, because the anodic reaction is depressed steadily as the inhibitor was added, whereas the copper cathodic reaction does not change. The corrosion of copper is mainly charge transfer controlled. On the other hand, according to the EIS measurements, the surface of copper is negatively charged in NaCl solution. The adsorption of the inhibitor on the copper surface takes place mainly through electrostatic interactions as well as charge sharing or transfer between the inhibitor molecules and the metal surface. Finally, the protection effect of SeAP remains good over time when immersion into corrosive media is applied, which shows that the inhibitor molecules tightly adsorb to the copper surface, and form a very stable and protective film on the surface.

REFERENCES

AAbd El Maksoud, S. Studies on the effect of pyranocoumarin derivatives on the corrosion of iron in 0.5 M HCl, *Corros. Sci*., 44,2002,803–813.

Ahamad, I. and Quraishi, M.A. Bis(benzimidazol-2-yl) disulphide: An efficient water soluble inhibitor for corrosion of mild steel in acid media, *Corros. Sci.*, 51; 2009, 2006–2013.

Ahmadi, M. Guinel, M.J.F., Synthesis, characterization and understanding of the mechanisms of electroplating of nanocrystalline–amorphous nickel–tungsten alloys using in situ electrochemical impedance spectroscopy,

Aljourani, J. Raeissi, K. and Golozar, M.A. Benzimidazole and its derivatives as corrosion inhibitors for mild steel in 1M HCl solution, *Corros. Sci*., 51 ,2009,1836–1843.

Behpour, M. Ghoreishi, S.M. Soltani, N. and Salavati-Niasari, M. The inhibitive effect of some bis-N,S-bidentate. Schiff bases on corrosion behaviour of 304 stainless steel in hydrochloric acid solution, *Corros. Sci*., 51,2009,1073–1082.

Bockris, J.O.M. and Reddy, A.K.N,. Modern Electrochemistry, Vol. 2, Plenum Publishing Corporation, 227 West 1t7th, Street, New York, 1976.

Chetouani, A. Aouniti, A. Hammouti, B. Benchat, N. Benhadda, T. and Kertit, S. Corrosion inhibitors for iron in hydrochloride acid solution by newly synthesisedpyridazine derivatives, *Corros. Sci.*, 45,2003, 1675–1684.

D.K.Yadav, M.A.Quraishi, B.Maiti, Inhibition effect of some benzylidenes on mild steel in 1 M HCl: An experimental and theoretical correlation, *Corros. Sci*., 55,2012, 254–266.

D.K.Yadav, M.A.Quraishi, B.Maiti, Inhibition effect of some benzylidenes on mild steel in 1 M HCl: An experimental and theoretical correlation, *Corros. Sci*., 55, 2012, 254–266.

Doner, A. and Kardas, G. N-Aminorhodanine as an effective corrosion inhibitor for mild steel in 0.5 M H_2SO_4, *Corros. Sci*., 53, 2011,4223–4232.

Doner, A. Sahin, E.A Kardas, G. and Serindag, O. Investigation of corrosion inhibition effect of 3-[(2-hydroxy-benzylidene)-amino]-2-thioxo-thiazolidin-4-one on corrosion of mild steel in the acidic medium, *Corros. Sci*., 66, 2013, 278–284.

Fragoza-Mar, L.F. Olivares-Xometl, O. Dominguez-Aguilar, M.A Flores, E.A. Arellanes-Lozada, P. Jimenez-Cruz, F. Corrosion inhibitor activity of 1,3-diketone malonates for mild steel in aqueous hydrochloric acid solution, *Corros. Sci*., 61,2012,171–184.

Garza, M., Liu, J., Magtoto, N.P. and Kelber, J.A. Adhesion behavior of electroless deposited Cu on Pt/Ta silicate and Pt/SiO_2, *Appl. Surf. Sci*., 222,2004,253–262.

Hamani, H. Douadi, T. Al-Noaimi, M. Issaadi, S. Daoud, D. Chafaa, S. Electrochemical and quantum chemical studies of some azomethine compounds as corrosion inhibitors for mild steel in 1 M hydrochloric acid, *Corros. Sci*., 88, 2014, 234-245.

J Alloy.Compd,574,2013,205

Keles, H., Keles, M., Dehri, I. and Serindag, O. The inhibitive effect of 6-amino-m-cresol and its Schiff base on the corrosion of mild steel in 0.5 M HCI medium, *Mater. Chem. Phys*., 112,2008 173–179.

Khaled, K.F. and Hackerman, N. Investigation of the inhibitive effect of ortho-substituted anilines on corrosion of iron in 1 M HCl solutions, *Electrochim. Acta*., 48,2003,2715–2723.

Kosari, A. Moayed, M.H. Davoodi, A. Parvizi, R. Momeni, M. Eshghi, H. and Moradi, H. Electrochemical and quantum chemical assessment of two organic compounds from pyridine derivatives as corrosion inhibitors for mild steel in HCl solution under stagnant condition and hydrodynamic flow. *Corros. Sci*., 78,2014,138-150.

Kumaraguru, S.P., Veeraraghavan, B. and Popov, B.N. Development of an Electroless Method to Deposit Corrosion-Resistant Silicate Layers on Metallic Substrates, *J. Electrochem. Soc*., 153,2006., B253–B259.

Lee, J., Kim, Y. and Chung, W. Effect of Ar bubbling during plasma electrolytic oxidation of AZ31B magnesium alloy in silicate electrolyte, *Appl. Surf. Sci*., 259,2012,454–459.

Li Xianghong, XieXiaoguang, Deng Shuduan and Du Guanben, Two phenylpyrimidine derivatives as new corrosion inhibitors for cold rolled steel in hydrochloric acid solution. *Corros. Sci*., 87,2014,27-39.

Li, X., Deng, S. and Fu, H. Inhibition of the corrosion of steel in HCl, H_2SO_4 solutions by bamboo leaf extract, *Corros. Sci*., 62 ,2012,163–175.

Lilja, M., Buttb, U., Shen, Z. and Bjorn, D. Nucleation and growth of hydroxyapatite on arc-deposited TiO_2surfaces studied by quartz crystal microbalance with dissipation, *Appl. Surf. Sci*., 284, 2013,1– 6.

Motamedi, M. Tehrani-Bagha, A.R. Mahdavian, M. Effect of aging time on corrosion inhibition of cationic surfactant on mild steel in sulfamic acid cleaning solution, *Corros. Sci*., 70, 2013, 46–54.

Nam, N.D., Somers, A., Mathesh, M., Seter, M., Hinton, B., Forsyth, M. and Tan, M.Y.J. The behaviour of praseodymium 4-hydroxycinnamate as an inhibitor for carbon dioxide corrosion and oxygen corrosion of steel in NaCl solution, *Corros. Sci*., 80,2014, 128-138.

Nilsson, S. and Björefors, F. Robinson, N.D. Electrochemical quartz crystal microbalance study of polyelectrolyte film growth under anodic conditions, *Appl. Surf. Sci*., 280 ,2013. 783– 790.

Obot, I.B., Obi-Egbedi, N.O. and Umoren, S.A. Antifungal drugs as corrosion inhibitors for aluminium in 0.1 M HCl, *Corros. Sci*., 51,2009,. 1868–1875.

Ongun, Y. Mer, B. D. Gülfeza, K. and Birgül, Y. Electrochemical and quantum chemical studies of 2-amino-4-methyl-thiazole as corrosion inhibitor for mild steel in HCl solution, *Corros. Sci*., 83,2014, 310-316.

Orazem, M.E. Pébère, N. and Tribollet, B. Enhanced Graphical Representation of Electrochemical Impedance Data, *J. Electrochem. Soc*, 153,2006, B129–B136

Pintado, S., Rodríguez-Amaro, R., Mayén, M. and Miguel-Rodríguez-Mellado, J. Electrochemical determination of the Glyphosate Metabolite Aminomethylphosphonic Acid (AMPA) in drinking Waters with an Electrodeposited Copper ElectrodeInt. *J. Electrochem. Sci*., 7,2012,305-312.

Quraishi, M.A. and Rawat, J. Inhibition of mild steel corrosion by some macrocyclic compounds in hot and concentrated hydrochloric acid, *Mater. Chem. Phys*., 73 ,2002, 118–122.

Sassi, W. Dhouibi, L. Berçot, P. Rezrazi, M. Triki, E. Effect of pyridine on the electrocrystallization and corrosion behavior of Ni–W alloy coated from citrate–ammonia media, *Appl. Surf. Sci*., 263 ,2012,373-381.

Sassi, W. Dhouibi, L. Berçot, P. Rezrazi, M. Triki, E. Study of the electroplating mechanism and physicochemical proprieties of deposited Ni-W-Silicate composite alloy, *Electrochim. Acta*., 117, 2014,443-452.

Simka, W. Socha, R.P. Dercz, G. Michalska, J. Maciej, A. Krzakała, A. Anodic oxidation of Ti–13Nb–13Zr alloy in silicate solutions, *Appl. Surf. Sci*., 279,2013, 317–323.

Solmaz, R. Altunbas, E. and Kardas, G. Investigation of adsorption and corrosion inhibition effect of 1,1'-thiocarbonyldiimidazole on mild steel in hydrochloric acid solution, *Prot. Met. Phys. Chem*., 47,2011, 262–269.

Solmaz, R. Kardas, G. Yazıcı, B.. Erbil, M. Adsorption and corrosion inhibitive properties of 2-amino-5-mercapto-1, 3, 4-thiadiazole on mild steel in hydrochloric acid media, *Colloid Surf*., A ; 312,2008, 7–17.

Solmaz, R. Kardas, G. Yazıcı, B. Erbil, M. Investigation of adsorption and inhibitive effect of 2-mercaptothiazoline on corrosion of mild steel in hydrochloric acid media, *Electrochim. Acta*, 53,2008,5941–5952.

Solmaz, R. Kardas, G. Yazıcı, B. Erbil, M., The Rhodanine inhibition effect on the corrosion of a mild steel in acid along the exposure time, Prot. Metals 5,2007, 476–482.

Solmaz, R. Mert, M.E. Kardas, G. Yazıcı, B. and Erbil, M. Adsorption and corrosion inhibition effect of 1, 1′-thiocarbonyldiimidazole on mild steel in H_2SO_4 solution and synergistic effect of iodide ion, *Acta Phys. Chim. Sin*., 24,2008,1185–1191.

Solmaz, R. Sahin, E.A. Doner, A. Kardas, G. The investigation of synergistic inhibition effect of rhodanine and iodide ion on the corrosion of copper in sulphuric acid solution, *Corros. Sci*., 53,2011, 3231–3240.

Solmaz, R., Kardas, G., Yazıcı, B. and Erbil, M., Inhibition effect of rhodanine for corrosion of mild steel in hydrochloric acid solution, Prot. Metals 41,2005. 581–585.

Song, Y.K. and Mansfeld, F. Development of a Molybdate–Phosphate–Silane–Silicate (MPSS) coating process for electrogalvanized steel, *Corros. Sci*., 48,2006,154–164.

Sowards, J. W. and Mansfield, E. Corrosion of copper and steel alloys in a simulated underground storage-tank sump environment containing acid-producing bacteria, *Corros. Sci.*, 87,2014. 460-471.

Tansuğ, G., Tüken, T., Giray, E.S., Fındıkkıran, G., Sığırcık, G., Demirkol, O. and Erbil, M. A new corrosion inhibitor for copper protection, *Corros. Sci*., 84,2014. 21-29.

Wu, T.H., Liao, S.C., Chen, Y.F., Huang, Y.Y., Wei, Y.S., Tu, S.J. and Chen, K.S. Determination of functionalized gold nanoparticles incorporated in hydrophilic and hydrophobic microenvironments by surface modification of quartz crystal microbalance. *Appl. Surf. Sci.,* 274 ,2013,418– 424.

Zargouni, Y. Sassi, W and Alouani, K. Corrosion inhibition of AISI 316L and modified-AISI 630 stainless steel by the new organic inhibitor $[(CH_3)_2N]_3PSe$ in chloride media: Electrochemical and physical study, *Mediter.J. Chem*., 4(2), 2015,105-110.

Zarrouk, A. Hammouti, B. Zarrok, H. Bouachrine, M. Khaled, K.F. Al-Deyab, S.S. Corrosion Inhibition of Copper in Nitric Acid Solutions Using New Triazole Derivative, *Int. J. Electrochem. Sci*., 7,2012,89-105.

Zhaoa, C. and Jiang, Z. Polymerization and redox behavior of polypyrrole (PPy) films by in situ EQCM and PT techniques, *Appl. Surf. Sci*., 229, 2004. 372–376.

****